

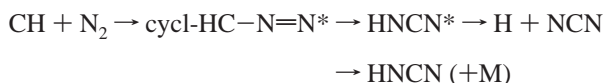
Ab Initio Chemical Kinetics for the OH + HNCN Reaction<sup>†</sup>Shucheng Xu<sup>\*,‡</sup> and M. C. Lin<sup>\*,§</sup>*Department of Chemistry, Emory University, Atlanta, Georgia 30322, and Institute of Molecular Science, Department of Applied Chemistry, National Chiao Tung University, Hsichu, Taiwan 300**Received: December 29, 2006; In Final Form: May 17, 2007*

The kinetics and mechanism of the reaction of the cyanomidyl radical (HNCN) with the hydroxyl radical (OH) have been investigated by ab initio calculations with rate constants prediction. The single and triplet potential energy surfaces of this reaction have been calculated by single-point calculations at the CCSD(T)/6-311+G(3df,2p) level based on geometries optimized at the B3LYP/6-311+G(3df,2p) and CCSD/6-311++G(d,p) levels. The rate constants for various product channels in the temperature range of 300–3000 K are predicted by variational transition-state and Rice–Ramsperger–Kassel–Marcus (RRKM) theories. The predicted total rate constants can be represented by the expressions  $k_{\text{total}} = 2.66 \times 10^{+2} \times T^{-4.50} \exp(-239/T)$  in which  $T = 300\text{--}1000$  K and  $1.38 \times 10^{-20} \times T^{2.78} \exp(1578/T) \text{ cm}^3 \text{ molecule}^{-1} \text{ s}^{-1}$  where  $T = 1000\text{--}3000$  K. The branching ratios of primary channels are predicted:  $k_1$  for forming singlet HON(H)CN accounts for 0.32–0.28, and  $k_4$  for forming singlet HONCNH accounts for 0.68–0.17 in the temperature range of 300–800 K.  $k_2 + k_7$  for producing  $\text{H}_2\text{O} + \text{NCN}$  accounts for 0.55–0.99 in the high-temperature range of 800–3000 K. The branching ratios of  $k_3$  for producing  $\text{HCN} + \text{HNO}$ ,  $k_6$  for producing  $\text{H}_2\text{N} + \text{NCO}$ ,  $k_8$  for forming  $^3\text{HN}(\text{OH})\text{CN}$ ,  $k_9$  for producing  $\text{CNOH} + ^3\text{NH}$ , and  $k_5 + k_{10}$  for producing  $\text{NH}_2 + \text{NCO}$  are negligible. The rate constants for key individual product channels are provided in a table for different temperature and pressure conditions.

## Introduction

The cyanomidyl radical (HNCN) is a reactive transient species that plays an important role in a variety of chemical environments, including prompt NO formation in hydrocarbon combustion, interstellar chemistry, and primordial reactions leading to the synthesis of amino acids from simple inorganic compounds. Experimentally, the HNCN radical was first identified spectroscopically by Herzberg and Warsop in 1963.<sup>1</sup> More recently, Wu et al.<sup>2</sup> probed the  $B^2A' \leftarrow X^2A''$  transition with laser-induced fluorescence, Yamamoto and Saito<sup>3</sup> reported the microwave spectrum of HNCN, and Clifford et al.<sup>4</sup> studied the photoelectron spectrum of the HNCN<sup>-</sup> ion. In 2001, the photodissociation spectroscopy and dynamics of the HNCN radical were investigated by Bise et al.<sup>5</sup>

Theoretically, ab initio calculations of the molecular geometry and vibrational frequencies of the HNCN ground state were first made by Tao et al. in 1994,<sup>6</sup> and then more recently by Puzzarini et al. in 2005.<sup>7</sup> In this laboratory, we first proposed HNCN to be the key stable intermediate of the new prompt NO formation reaction by  $\text{CH} + \text{N}_2$  along a spin-allowed doublet electronic state path:<sup>8</sup>



where  $\text{cycl-HC-N=N}^*$  includes two cyclic isomers and “\*” denotes internal excitation. Under high-pressure combustion conditions, the collisional stabilization of the excited HNCN

by the second step given above may provide a high concentration of HNCN radicals.

The reaction of HNCN with OH should therefore play an important role in the oxidation of HNCN, producing prompt NO precursors such as NCN, HNO, and HCN. In the literature, there have been no reports on the kinetics and mechanism for the reaction of OH with HNCN experimentally or theoretically. In this work, the singlet and triplet potential energy surfaces (PESs) of the OH + HNCN reaction have been calculated at the CCSD(T)/6-311+G(3df,2p) level of theory. In addition, the rate constants and branching ratios for the primary reaction channels in the temperature range of 300–3000 K have been predicted for combustion modeling applications.

## Computational Methods

The optimized geometries of the reactants, transition states, intermediate complexes, and products for the reaction of OH + HNCN have been calculated at the B3LYP/6-311+G(3df,2p) level. In addition, the optimized geometries of primary channels for singlet PESs and triplet PESs for this reaction have been calculated at the higher CCSD/6-311++G(d,p) level in addition to B3LYP/6-311+G(3df,2p). The energies for the singlet and triplet PESs are improved by single-point calculations at the CCSD(T)/6-311+G(3df,2p) level of theory based on the optimized geometries at the B3LYP/6-311+G(3df,2p) and CCSD/6-311++G(d,p) levels, which have been performed successfully for the reaction of OH +  $\text{CH}_2\text{O}$ .<sup>9</sup>

The rate constants for the key product channels were computed with variational transition-state theory (TST) and Rice–Ramsperger–Kassel–Marcus (RRKM) theory using the VariFlex code.<sup>10</sup> All quantum chemistry calculations were carried out by the Gaussian 03<sup>11</sup> package using a PC cluster

<sup>†</sup> Part of the special issue “M. C. Lin Festschrift”.

\* Corresponding author. E-mail: sxu@emory.edu.

<sup>‡</sup> Emory University.<sup>§</sup> National Chiao Tung University.

and the computers at the Cherry L. Emerson Center for Scientific Computation at Emory University.

## Results and Discussion

**1. PESs and the Reaction Mechanism.** The optimized geometries for the species involved in the reaction of OH with HNCN at the B3LYP/6-311+G(3df,2p) and CCSD/6-311++G(d,p) (data in parenthesis) levels are shown in Figure 1. The parameters of optimized geometries using both the B3LYP and CCSD methods are close to each other except for the distance of HO–HNCN in *t*-TS<sub>1</sub>. The energies for all the species obtained by the CCSD(T)/6-311+G(3df,2p)//B3LYP/6-311+G(3df,2p), and CCSD(T)/6-311+G(3df,2p)//CCSD/6-311++G(d,p) methods are listed in Table 1. On average, the relative energies for the species using the CCSD geometries were found to be about 0.4 kcal/mol higher than those using the B3LYP geometries. The reaction of OH with HNCN can occur on both singlet and triplet PESs. For the singlet PES, it was found to be very complicated because of the existence of the resonance structures:  $\text{HN}-\text{C}\equiv\text{N} \leftrightarrow \text{HN}=\text{C}=\text{N}$ , which give rise to 3 association complexes with 14 isomerization channels and 15 dissociation processes, producing 19 products. For the triplet PES, it was found that there was one hydrogen abstraction channel and two addition channels. We discuss the PESs and reaction mechanism in the following four sections (1a, 1b, 1c, and 1d). In order to simplify the discussion of the singlet and triplet PESs, we only mention the energies using the B3LYP geometries in these sections because the energies using the CCSD geometries are close to those using the B3LYP geometries, as listed in Table 1 and shown in parentheses in Figure 2a–c.

**1a. Formation and Isomerization of Singlet Intermediates.** As shown in Scheme 1 and Figure 2a, the reaction of OH with HNCN first forms primary intermediates *trans*-HON(H)CN (denoted as *t*-HON(H)CN; dihedral angle HONC = 118.8°) with a binding energy of 46.9 kcal/mol, *cis*-HON(H)CN (denoted as *c*-HON(H)CN; dihedral angle HONC = –56.3°) with a binding energy of 44.2 kcal/mol when the OH attacks the N atom next to H, and also forms HONCNH with a binding energy of 41.4 kcal/mol when the OH associates with the terminal N atom.

As shown in Scheme 1, *t*-HON(H)CN and *c*-HON(H)CN are two conformers of HON(H)CN and can transform to each other by an internal rotation about the O–N bond via TS<sub>19</sub> (dihedral angle HONC = –132.3°) with a barrier of 6.9 kcal/mol. HON(H)CN can also isomerize to HONCNH via TS<sub>20</sub> with a barrier of 68.2 kcal/mol. Furthermore, HON(H)CN and HONCNH can isomerize to nine other intermediates. For example, *t*-HON(H)CN can transform to ON(H<sub>2</sub>)CN via TS<sub>3</sub> with a barrier of 56.7 kcal/mol or to *t*-ONC(H)NH via TS<sub>4</sub> with a barrier of 71.1 kcal/mol. HONCNH can isomerize to *t*-NC(NH)OH via TS<sub>9</sub> with a barrier of 39.9 kcal/mol or to ON(H)CNH via TS<sub>13</sub> with a barrier of 59.8 kcal/mol. Similarly, *t*-ONC(H)NH can transform to *c*-ONC(H)NH via TS<sub>8</sub> with a barrier of 25.1 kcal/mol or to ONCNH<sub>2</sub> via TS<sub>6</sub> with a barrier of 73.6 kcal/mol, and *t*-NC(NH)OH can transform to *c*-NC(NH)OH via TS<sub>11</sub> with a barrier of 5.2 kcal/mol or *t*-HOCNNH via TS<sub>10</sub> with a barrier of 50.0 kcal/mol. In addition, *c*-NC(NH)OH can transform to *c*-HOCNNH through TS<sub>12</sub> with a barrier of 53.4 kcal/mol, and ON(H)CNH can transform to *t*-ONC(H)NH TS<sub>17</sub> with a barrier of 36.1 kcal/mol or to *c*-ONC(H)NH through TS<sub>14</sub> with a barrier of 33.0 kcal/mol. These isomerization reactions can also occur reversely, as one would expect.

**1b. Primary Singlet Product Channels.** As shown in Figure 2a, the OH + HNCN reaction may generate the following

primary products with predicted enthalpy changes: H<sub>2</sub>O + <sup>1</sup>NCN ( $\bar{a}^1\Delta_g$ ), –4.8 kcal/mol; HCN + HNO, –28.3 kcal/mol; HNC + HNO, –14.6 kcal/mol; and H<sub>2</sub>N + NCO, –11.6 kcal/mol. The <sup>1</sup>NCN product is formed by H<sub>2</sub>O elimination from the primary intermediates, *t*-HON(H)CN and *c*-HON(H)CN, by overcoming the barriers of 49.4 kcal/mol at TS<sub>1</sub> and 49.3 kcal/mol at TS<sub>2</sub>. The <sup>1</sup>NCN ( $\bar{a}^1\Delta_g$ ) product is the first excited state of NCN, which is predicted to be higher than the ground state  $\tilde{X}^3\Sigma_g^-$  by 30.1 kcal/mol at both the CCSD(T)//B3LYP and CCSD levels; the value is close to the previously predicted 30.7 kcal/mol calculated using the ROHF-CCSD(T)/pVTZ method by Martin et al.,<sup>12</sup> and 28.8 kcal/mol calculated using the CBS-QCI/APNO method by Clifford et al.<sup>4</sup> These values are clearly higher than the reported experimental result of  $23.2 \pm 0.2$  kcal/mol.<sup>13,14</sup> As the CCSD(T) is a single-reference method, we also performed a large-scale multireference calculation for the ( $\bar{a}^1\Delta_g - \tilde{X}^3\Sigma_g^-$ ) energy difference using the CASPT2(8,8)/6-311+G(3df,2p) method based on the geometries optimized at the CASSCF(8,8)/6-311+G(3df,2p) level. Here we selected eight active electrons of  $3\sigma_g^2 1\pi_\mu^4 1\pi_g^2$  and eight active orbitals for both states ( $1\sigma_g^2 1\sigma_u^2 2\sigma_g^2 3\sigma_g^2 2\sigma_u^2 4\sigma_g^2 3\sigma_u^2 1\pi_\mu^4 1\pi_g^2$ ). The predicted value is 29.4 kcal/mol, which is very close to the ones obtained by the single-reference methods cited above, but is noticeably higher than the 23.2 kcal/mol experimental result.

In addition, the products HCN + HNO may be produced by the dissociation of intermediates *t*-HON(H)CN, ON(H<sub>2</sub>)CN, and *t*-ONC(H)NH via TS<sub>21</sub> with a barrier of 87.2 kcal/mol, TS<sub>18</sub> with a barrier of 23.0 kcal/mol, and TS<sub>7</sub> with a barrier of 75.4 kcal/mol, respectively. Furthermore, the products HNC + HNO may be produced by the dissociation of ON(H)CNH via TS<sub>15</sub> with a barrier of 19.2 kcal/mol. Similarly, the H<sub>2</sub>N + NCO products may be formed by the dissociation of *t*-NC(NH)OH via TS<sub>16</sub> with a barrier of 47.6 kcal/mol.

The predicted heats of reaction for the formation of H<sub>2</sub>O + <sup>3</sup>NCN (–34.9 kcal/mol at both the CCSD(T)//B3LYP and CCSD(T)//CCSD levels), HCN + HNO (–28.3 kcal/mol at both the CCSD(T)//B3LYP and CCSD(T)//CCSD levels), and HNC + HNO (–14.6 kcal/mol at the CCSD(T)//B3LYP and –13.8 kcal/mol at the CCSD(T)//CCSD level) from OH + HNCN listed in Table 1 are in reasonable agreement with the available experimental values at 0 K (–30.7 ± 4.0 kcal/mol, –25.8 ± 2.4 kcal/mol, and –12.4 ± 1.9 kcal/mol, respectively), based on  $\Delta_f H_0(\text{OH}) = 8.87 \pm 0.07$  kcal/mol,<sup>15</sup>  $\Delta_f H_0(\text{HNCN}) = 72.3 \pm 0.7$  kcal/mol,<sup>5</sup>  $\Delta_f H_0(\text{H}_2\text{O}) = -57.10 \pm 0.01$  kcal/mol,<sup>15</sup> and  $\Delta_f H_0(^3\text{NCN}) = 107.6 \pm 3.2$  kcal/mol derived from  $\Delta_f H_{298}(^3\text{NCN}) = 107.7 \pm 3.2$  kcal/mol,<sup>4</sup>  $\Delta_f H_0(\text{HCN}) = 30.9 \pm 0.7$  kcal/mol,<sup>5</sup>  $\Delta_f H_0(\text{HNCN}) = 44.3 \pm 0.9$  kcal/mol,<sup>5</sup> and  $\Delta_f H_0(\text{HNO}) = 24.5$  kcal/mol.<sup>16</sup> For <sup>3</sup>NCN, Bise et al. obtained an experimental value of  $\Delta_f H_0(^3\text{NCN}) = 111.4 \pm 0.7$  kcal/mol.<sup>13</sup> This value would give rise to the experimental heat of reaction for H<sub>2</sub>O + <sup>3</sup>NCN formation, –26.8 ± 1.5 kcal/mol, which is 8.1 kcal/mol higher than the predicted result.

**1c. Secondary Singlet Product Channels.** As shown in Figure 2b, the OH + HNCN reaction may produce the following minor products with predicted enthalpy changes: H<sub>2</sub> + ONCN, –9.4 kcal/mol; NO + *t*-HNCH, 1.3 kcal/mol; HNN + HOC, 25.7 kcal/mol; HNC + HON, 27.6 kcal/mol; CN + *c*-HNOH, 43.7 kcal/mol; CN + *t*-HNOH, 48.9 kcal/mol; and H<sub>2</sub>N + CNO, 51.0 kcal/mol. The H<sub>2</sub> + ONCN products may be formed by the dissociation of the intermediate ON(H<sub>2</sub>)CN by overcoming the barrier of 46.3 kcal/mol at TS<sub>5</sub>. The products NO + *t*-HNCH may be produced by the direct barrierless

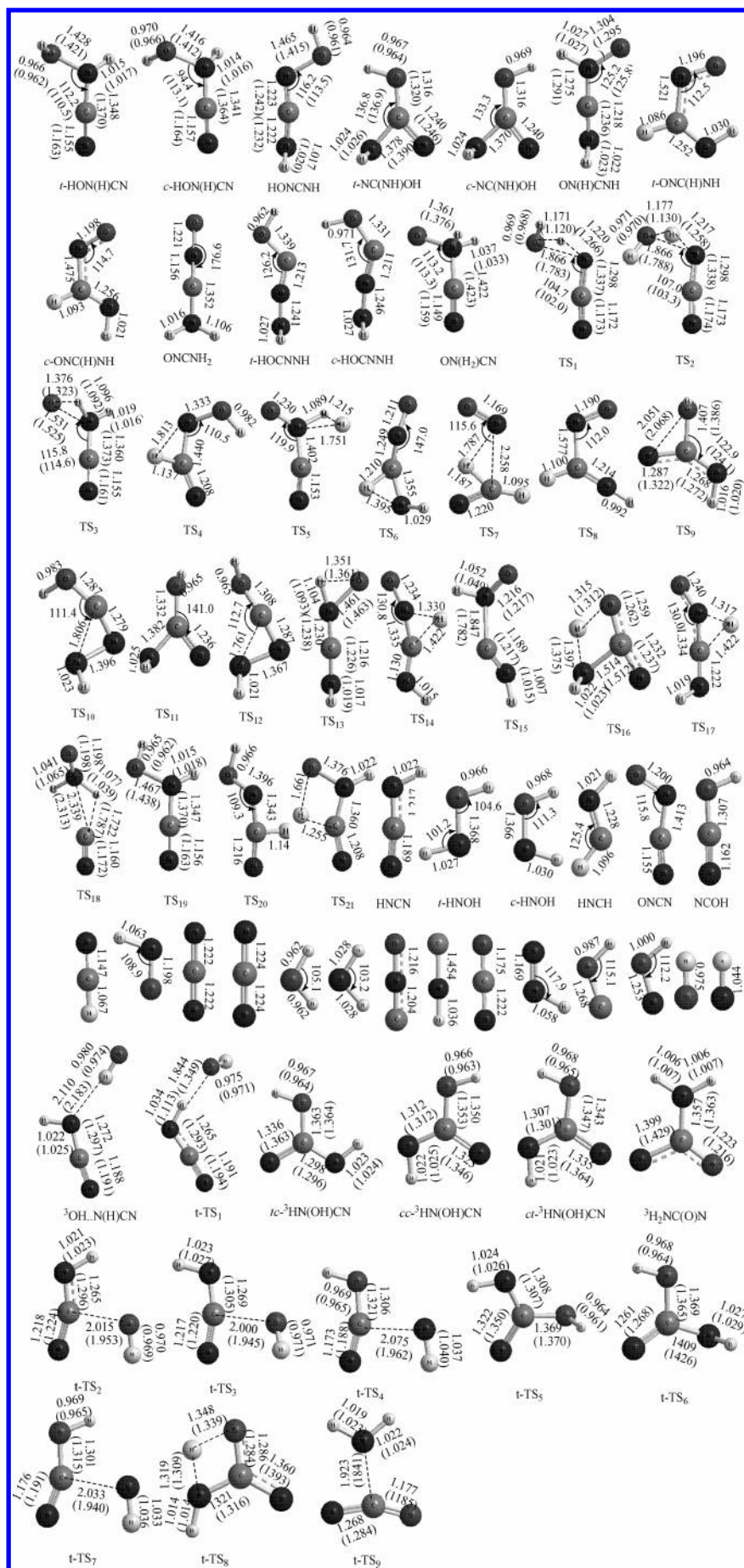


**Figure 1.** Optimized geometries of the reaction  $\text{OH} + \text{HNCN}$  computed at the B3LYP/6-311+G(3df,2p) and CCSD/6-311++G(d,p) (data in parenthesis) levels.

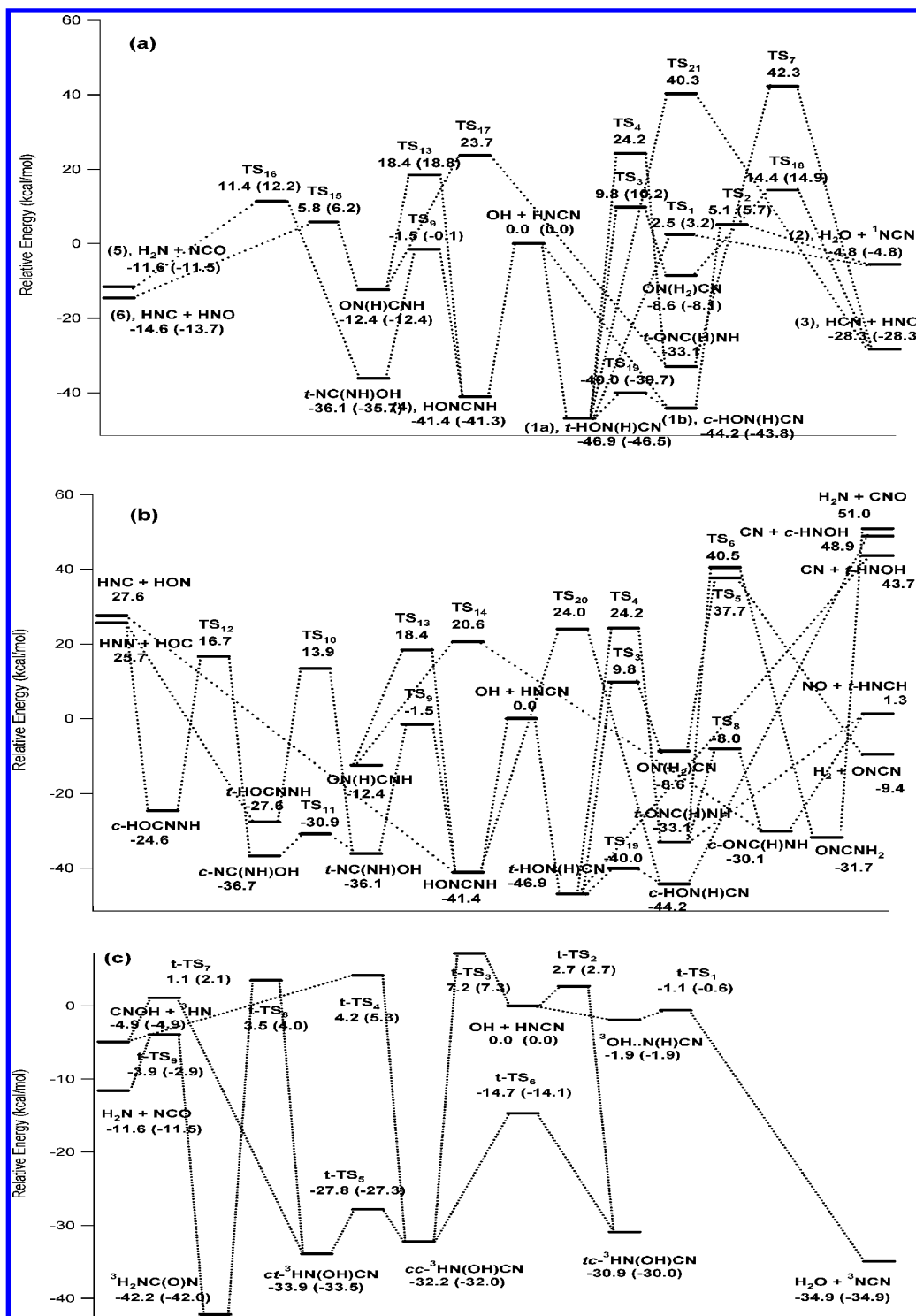
TABLE 1: Total and Relative Energies<sup>a</sup> of Reactants, Transition States, and Products of the Reaction OH + HNCN

species or reactions	B3LYP/6-311+G(3df,2p)		CCSD(T) <sup>b</sup> /6-311+G(3df,2p)	CCSD(T) <sup>c</sup> /6-311+G(3df,2p)	$\Delta H_{0,\text{expt}}^d$
	ZPE	energies	B3LYP/6-311+G(3df,2p)	CCSD/6-311++G(d,p)	
OH + HNCN	0.028085	-223.923551	-223.497423	-223.497792	(0.0)
<i>t</i> -HON(H)CN	6.7	-41.3	-46.9	-46.5	
<i>c</i> -HON(H)CN	6.5	-39.0	-44.2	-43.8	
HONCNH	6.0	-40.6	-41.4	-41.3	
<i>t</i> -NC(NH)OH	6.3	-28.6	-36.1		
<i>c</i> -NC(NH)OH	6.4	-29.1	-36.7	-36.2	
ON(H)CNH	5.7	-13.4	-12.4	-12.4	
<i>t</i> -ONC(H)NH	5.7	-25.4	-33.1		
<i>c</i> -ONC(H)NH	5.6	-22.9	-30.1		
ONCNH <sub>2</sub>	5.9	-32.1	-31.7		
<i>t</i> -HOCNNH	6.3	-26.4	-27.6		
<i>c</i> -HOCNNH	5.9	-23.0	-24.6		
ON(H <sub>2</sub> )CN	6.6	-2.4	-8.6	-8.1	
TS <sub>1</sub>	1.7	4.8	2.5	3.2	
TS <sub>2</sub>	1.6	7.5	5.1	5.7	
TS <sub>3</sub>	3.8	14.7	9.8	10.2	
TS <sub>4</sub>	2.8	32.9	24.2		
TS <sub>5</sub>	0.1	44.8	37.7		
TS <sub>6</sub>	1.9	39.3	40.4		
TS <sub>7</sub>	-0.1	49.0	42.3		
TS <sub>8</sub>	3.8	-2.9	-8.0		
TS <sub>9</sub>	4.2	0.6	-1.5	-0.1	
TS <sub>10</sub>	4.3	20.6	13.9		
TS <sub>11</sub>	5.5	-22.7	-30.8		
TS <sub>12</sub>	4.3	22.1	16.6		
TS <sub>13</sub>	2.0	16.4	18.4	18.8	
TS <sub>14</sub>	1.8	19.3	20.6		
TS <sub>15</sub>	3.3	7.5	5.8	6.2	
TS <sub>16</sub>	2.1	17.0	11.4	12.2	
TS <sub>17</sub>	1.5	22.1	23.7		
TS <sub>18</sub>	3.1	17.3	14.4	14.9	
TS <sub>19</sub>	6.0	-34.6	-40.0	-39.7	
TS <sub>20</sub>	2.2	31.6	24.0		
TS <sub>21</sub>	1.5	51.2	40.3		
<sup>3</sup> OH...N(H)CN	1.6	-1.3	-1.9	-1.9	
<i>t</i> -TS <sub>1</sub>	1.8	-1.6	-1.1	-0.6	
<i>tc</i> - <sup>3</sup> HN(OH)CN	5.1	-28.2	-30.9	-30.5	
<i>cc</i> - <sup>3</sup> HN(OH)CN	5.3	-30.0	-32.2	-32.0	
<i>ct</i> - <sup>3</sup> HN(OH)CN	5.5	-31.2	-33.9	-33.5	
<sup>3</sup> H <sub>2</sub> NC(O)N	5.5	-39.6	-42.2	-42.0	
<i>t</i> -TS <sub>2</sub>	1.8	0.1	2.7	2.7	
<i>t</i> -TS <sub>3</sub>	1.7	4.7	7.2	7.3	
<i>t</i> -TS <sub>4</sub>	2.5	9.1	4.2	5.3	
<i>t</i> -TS <sub>5</sub>	4.6	-25.2	-27.8	-27.3	
<i>t</i> -TS <sub>6</sub>	4.2	-12.3	-14.7	-14.1	
<i>t</i> -TS <sub>7</sub>	2.8	5.2	1.1	2.1	
<i>t</i> -TS <sub>8</sub>	2.1	5.4	3.5	4.0	
<i>t</i> -TS <sub>9</sub>	2.2	-5.7	-3.9	-2.9	
H <sub>2</sub> O + <sup>1</sup> NCN	0.7	-0.9	-4.8	-4.8	
H <sub>2</sub> O + <sup>3</sup> NCN	1.1	-33.2	-34.9	-34.9	-30.7 ± 4.0
HCN + HNO	1.3	-19.2	-28.3	-28.3	-25.8 ± 2.4
HNC + HNO	0.2	-6.4	-14.6	-13.7	-12.4 ± 1.9
H <sub>2</sub> N + NCO	0.6	-11.7	-11.6	-11.5	
<sup>3</sup> NH + NCOH	0.6	2.3	-4.9	-4.9	
H <sub>2</sub> + ONCN	-3.0	-1.4	-9.4		
NO + <i>t</i> -HNCH	1.4	4.3	1.3		
HNN + HOC	-1.0	27.1	25.7		
HNC + HON	-0.1	33.8	27.6		
CN + <i>t</i> -HNOH	2.4	49.7	43.7		
CN + <i>c</i> -HNOH	2.0	54.7	48.9		
H <sub>2</sub> N + CNO	-0.1	50.7	51.0		

<sup>a</sup> Total energies for OH + HNCN are in a.u., and relative energies for others are in kcal mol<sup>-1</sup>. <sup>b</sup> Single-point energies based on optimized geometries calculated at the B3LYP/6-311+G(3df,2p) level. <sup>c</sup> Single-point energies based on optimized geometries calculated at the CCSD/6-311++G(d,p) level. <sup>d</sup> At 0 K,  $\Delta_f H_0$  values are as follows:  $\Delta_f H_0(\text{OH}) = 8.87 \pm 0.07$  kcal/mol,<sup>15</sup>  $\Delta_f H_0(\text{HNCN}) = 72.3 \pm 0.7$  kcal/mol,<sup>5</sup>  $\Delta_f H_0(\text{H}_2\text{O}) = -57.10 \pm 0.01$  kcal/mol,<sup>15</sup> and  $\Delta_f H_0(^3\text{NCN}) = 107.6 \pm 3.2$  kcal/mol, derived from  $\Delta_f H_{298}(^3\text{NCN}) = 107.7 \pm 3.2$  kcal/mol,<sup>4</sup>  $\Delta_f H_0(\text{HCN}) = 30.9 \pm 0.7$  kcal/mol,<sup>5</sup>  $\Delta_f H_0(\text{HON}) = 44.3 \pm 0.9$  kcal/mol,<sup>5</sup> and  $\Delta_f H_0(\text{HNO}) = 24.5$  kcal/mol.<sup>16</sup>

dissociation of *t*-ONC(H)NH and *c*-ONC(H)NH with dissociation energies of 44.4 and 41.4 kcal/mol, respectively. Similarly, the production of other radical product pairs takes place

by barrierless dissociation processes with the predicted endothermicities: HNN + HOC from *t*-HOCNNH and *c*-HOCNNH, 53.3 and 50.3 kcal/mol, respectively; HNC + HON

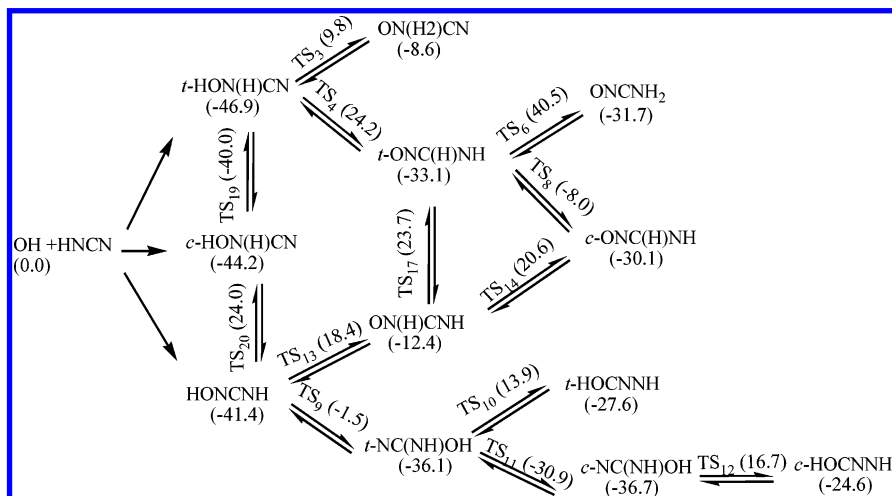


**Figure 2.** (a) Singlet PES of the primary product channels of OH + HNCN calculated at the CCSD(T)/6-311+G(3df,2p)//B3LYP/6-311+G(3df,2p) and CCSD(T)/6-311+G(3df,2p)//CCSD/6-311++G(d,p) (data in parenthesis) levels. (b) Singlet PES of the secondary product channels of OH + HNCN calculated at the CCSD(T)/6-311+G(3df,2p)//B3LYP/6-311+G(3df,2p) level. (c) Triplet PES of the reaction of OH + HNCN calculated at the CCSD(T)/6-311+G(3df,2p)//B3LYP/6-311+G(3df,2p) and CCSD(T)/6-311+G(3df,2p)//CCSD/6-311++G(d,p) (data in parenthesis) levels.

from HONCN, 69.0 kcal/mol; CN + *t*-HNOH from *t*-HON(H)CN, 90.6 kcal/mol; CN + *c*-HNOH from *c*-HON(H)CN, 93.1 kcal/mol, and, finally, H<sub>2</sub>N + CNO from ONCNH<sub>2</sub>, 82.7 kcal/mol.

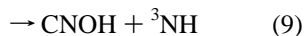
*1d. Triplet Product Channels.* As shown in Figure 2c, for the OH + HNCN reaction, we have found one triplet abstraction channel and two triplet addition channels. For the triplet abstraction channel, the reactants of OH radical with HNCN radical first form a triplet precomplex <sup>3</sup>OH...N(H)CN with a

1.9 kcal/mol binding energy, and the H-abstraction takes places via triplet *t*-TS<sub>1</sub> with a 0.7 kcal/mol barrier to produce the products H<sub>2</sub>O + <sup>3</sup>NCN ( $\tilde{X}^3\Sigma_g^-$ ). For the triplet addition channels, the reaction of OH with HNCN forms triplet intermediate *tc*-<sup>3</sup>HN(OH)CN with -30.9 kcal/mol exothermicity via triplet *t*-TS<sub>2</sub> with a 2.7 kcal/mol barrier or *cc*-<sup>3</sup>HN(OH)CN with -32.2 kcal/mol exothermicity via triplet *t*-TS<sub>3</sub> with a 7.2 kcal/mol barrier. *cc*-<sup>3</sup>HN(OH)CN can transform to *tc*-<sup>3</sup>HN(OH)CN by an internal rotation about the C–O bond via *t*-TS<sub>6</sub> with a barrier of 17.5

**SCHEME 1: Formation and Isomerization of Intermediates of OH + HNCN, Where Data in Parentheses Are Relative Energies in kcal/mol**

kcal/mol, and can also transform to another conformer  $ct$ - $^3\text{HN}(\text{OH})\text{CN}$  with  $-33.9$  kcal/mol exothermicity by an internal rotation about the C–N bond via  $t$ -TS<sub>5</sub> with a barrier of  $5.4$  kcal/mol. The intermediates  $cc$ - $^3\text{HN}(\text{OH})\text{CN}$  and  $ct$ - $^3\text{HN}(\text{OH})\text{CN}$  can dissociate to the products of singlet CNOH +  $^3\text{NH}$  with  $-4.9$  kcal/mol exothermicity via  $t$ -TS<sub>4</sub> with a barrier of  $36.4$  kcal/mol and  $t$ -TS<sub>7</sub> with a barrier of  $35.0$  kcal/mol, respectively. In addition,  $ct$ - $^3\text{HN}(\text{OH})\text{CN}$  can isomerize to another intermediate  $^3\text{H}_2\text{NC}(\text{O})\text{N}$  with  $-42.2$  kcal/mol exothermicity via  $t$ -TS<sub>8</sub> with a barrier of  $37.4$  kcal/mol. Furthermore,  $^3\text{H}_2\text{NC}(\text{O})\text{N}$  can dissociate to produce  $\text{H}_2\text{N} + \text{NCO}$  via  $t$ -TS<sub>9</sub> with a barrier of  $46.1$  kcal/mol. Interestingly, here we found that the geometries of all triplet intermediates are planar.

**2. Rate Constant Calculations for the Primary Reaction Channels of OH + HNCN.** *2a. Methods Employed for Rate Constant Calculations.* The rate constants for the following primary singlet and triplet reaction channels of OH + HNCN have been predicted by statistical calculations:



The rate constants for the reactions of OH with HNCN with the primary six singlet and four triplet channels have been calculated using variational TST and RRKM theory by the VariFlex Code<sup>10</sup> in the temperature range 300–3000 K with Ar as the bath gas. Channel 1 is an association reaction forming the intermediate HON(H)CN, whose two conformers,  $t$ -HON(H)CN and  $c$ -HON(H)CN, are treated as one intermediate via hindered rotation about the O–N bond with a barrier of  $6.9$

kcal/mol. Channel 2 is a dissociation reaction via the intermediate HON(H)CN and two dissociation paths by transition states TS<sub>1</sub> and TS<sub>2</sub> to produce the same  $\text{H}_2\text{O} + {}^1\text{NCN}$  products through the  $t$ - and  $c$ -conformers, respectively. Channel 3 is a dissociation reaction via the intermediate HON(H)CN and transition states TS<sub>3</sub> and TS<sub>18</sub> to produce the  $\text{HCN} + \text{HNO}$  products, where the primary controlling transition state TS<sub>18</sub> and secondary transition state TS<sub>3</sub> with a relatively shallow intermediate ON(H<sub>2</sub>)CN can be treated as a combined transition state by the multiple reflection treatment.<sup>9</sup> Channel 4 is an association reaction forming the intermediate HONCNH. Channel 5 is treated as a dissociation reaction to  $\text{H}_2\text{N} + \text{NCO}$  via the intermediate HONCNH and the primary transition state TS<sub>16</sub> because the barrier of TS<sub>16</sub> is  $13.0$  kcal/mol higher than that of the secondary transition state TS<sub>9</sub> lying  $-1.5$  kcal/mol below the reactants. Channel 6 is treated as a dissociation reaction to  $\text{HNC} + \text{HNO}$  via the intermediate HONCNH and the primary transition state TS<sub>13</sub> because the barrier of TS<sub>13</sub> is  $14.6$  kcal/mol higher than that of the exit transition state TS<sub>15</sub>.

Channel 7 is a triplet H-abstraction reaction through the precomplex  ${}^3\text{OH}\cdots\text{N}(\text{H})\text{CN}$  and the triplet transition state  $t$ -TS<sub>1</sub> to produce the  $\text{H}_2\text{O} + {}^3\text{NCN}$  products, where the energy of  $t$ -TS<sub>1</sub> is  $0.6$  kcal/mol lower than the reactants calculated at the CCSD(T)//CCSD level. The existence of the preassociation complex has been shown to have a significant effect on the predicted rate constants due to multiple reflections above the well of the complex in previous studies,<sup>9,17</sup> when the energy of an exit transition state is close to that of the reactants. Therefore, the effect of multiple reflections was examined for channel 7. Channel 8 is an association reaction forming the triplet intermediate  $tc$ - $^3\text{HN}(\text{OH})\text{CN}$  via  $t$ -TS<sub>2</sub> or its conformer  $cc$ - $^3\text{HN}(\text{OH})\text{CN}$  via  $t$ -TS<sub>3</sub>. Channel 9 is a dissociation reaction via the intermediate  $^3\text{HN}(\text{OH})\text{CN}$  and two dissociation paths by transition states  $t$ -TS<sub>4</sub> and  $t$ -TS<sub>7</sub> to produce the same CNOH +  $^3\text{NH}$  products. Channel 10 is treated as a dissociation reaction to  $\text{H}_2\text{N} + \text{NCO}$  via transition states  $t$ -TS<sub>3</sub>,  $t$ -TS<sub>8</sub>, and  $t$ -TS<sub>9</sub>, where  $t$ -TS<sub>9</sub> is treated as a secondary transition state of  $t$ -TS<sub>8</sub>. Although these treatments for channels 3, 5, and 6 may have systematic errors, they have negligible effects on the total rate constants because the values of the rate constants of channels 3, 5, and 6 are negligibly small, even at high temperatures, as will be discussed later. The rate constants for these channels are based on the molecular parameters, including the geometries, vibrational frequencies, and rotational constants calculated at

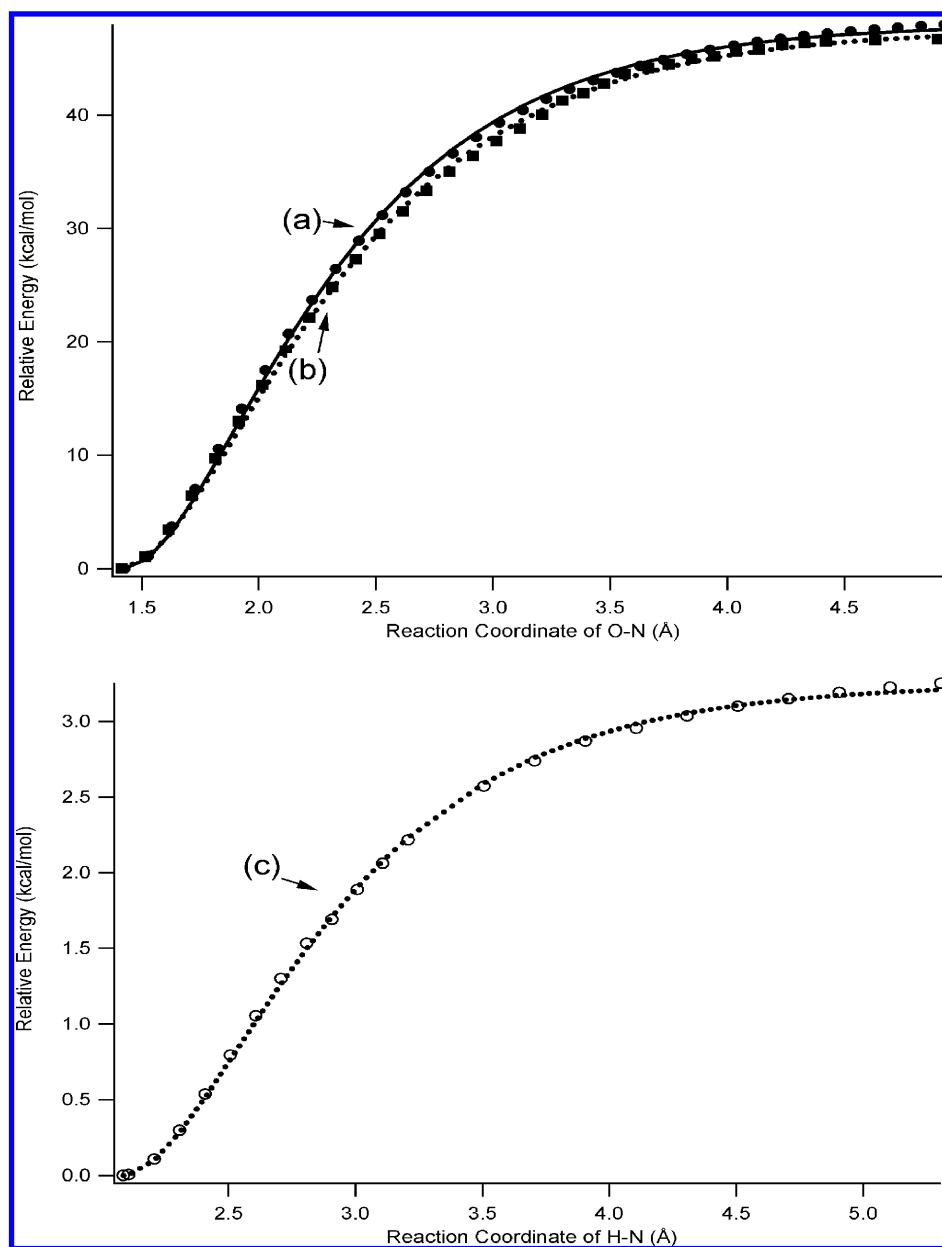


**Figure 3.** (a) MEPs (●) of OH + HNCN → HON(H)CN along the reaction coordinate of O–N calculated at the B3LYP/6-311+G(3df,2p) level with the fitted Morse curves (solid curve). (b) MEPs (■) of OH + HNCN → HONCNH along the reaction coordinate of O–N calculated at the B3LYP/6-311+G(3df,2p) level with the fitted Morse curves (dotted curve). (c) MEPs (○) of OH + HNCN → <sup>3</sup>OH···N(H)CN along the reaction coordinate of H–N calculated at the B3LYP/6-311+G(3df,2p) level with the fitted Morse curves (dotted curve).

the higher CCSD/6-311++G(*d,p*) level and the PESs calculated at the CCSD(T)/6-311+G(3df,2p) level listed in Table 1.

For the barrierless association processes OH + HNCN → HON(H)CN shown in Figure 3 a and OH + HNCN → HONCNH shown in Figure 3 b, the minimum energy paths (MEPs) for forming the primary intermediates, HON(H)CN and HONCNH, were obtained by computing the potential energy curves along the reaction coordinate from 1.5 to 5.0 Å with a step size of 0.1 Å estimated at the UB3LYP/6-311+G(3df,2p) level. Similarly, for the barrierless association processes OH + HNCN → triplet precomplex <sup>3</sup>OH···N(H)CN shown in Figure 3c, the MEP was obtained by computing the potential energy curves along the reaction coordinate from 2.1 to 5.0 Å with a step size of 0.1 Å at the UB3LYP/6-311+G(3df,2p) level. The calculated MEPs could be fitted to the Morse potential function with the parameters,  $\beta = 1.502 \text{ \AA}^{-1}$  with  $R_0 = 1.428 \text{ \AA}$  and  $D_e = 53.6 \text{ kcal/mol}$ ;  $\beta = 1.416 \text{ \AA}^{-1}$  with  $R_0 = 1.415 \text{ \AA}$  and  $D_e = 47.5 \text{ kcal/mol}$ ; and  $\beta = 1.573 \text{ \AA}^{-1}$  with  $R_0 = 2.109 \text{ \AA}$  and  $D_e$

$= 3.4 \text{ kcal/mol}$  for forming HON(H)CN, HONCNH, and triplet <sup>3</sup>OH···N(H)CN, respectively, where the energies for  $D_e$  were scaled at the CCSD(T)//CCSD level without ZPE corrections. For the variational rate constant calculations by the VariFlex code, a statistical treatment of the transitional-mode contributions to the transition-state partition functions was performed variationally. The numbers of state are evaluated according to the variable reaction coordinate flexible transition-state theory,<sup>10,18</sup> an energy grain size of 1.00  $\text{cm}^{-1}$  was used for the convolution of the conserved mode vibrations, and a grain size of 50.00  $\text{cm}^{-1}$  was used for the generation of the transitional-mode numbers of states. The estimate of the transitional-mode contribution to the transition-state number of states for a given energy is evaluated via Monte Carlo integration with 10 000 configuration numbers. The energy-transfer process was computed on the basis of the exponential down model with a  $\langle \Delta E \rangle_{\text{down}}$  value (the mean energy transferred per collision) of 400  $\text{cm}^{-1}$  for Ar. In order to achieve convergence in the

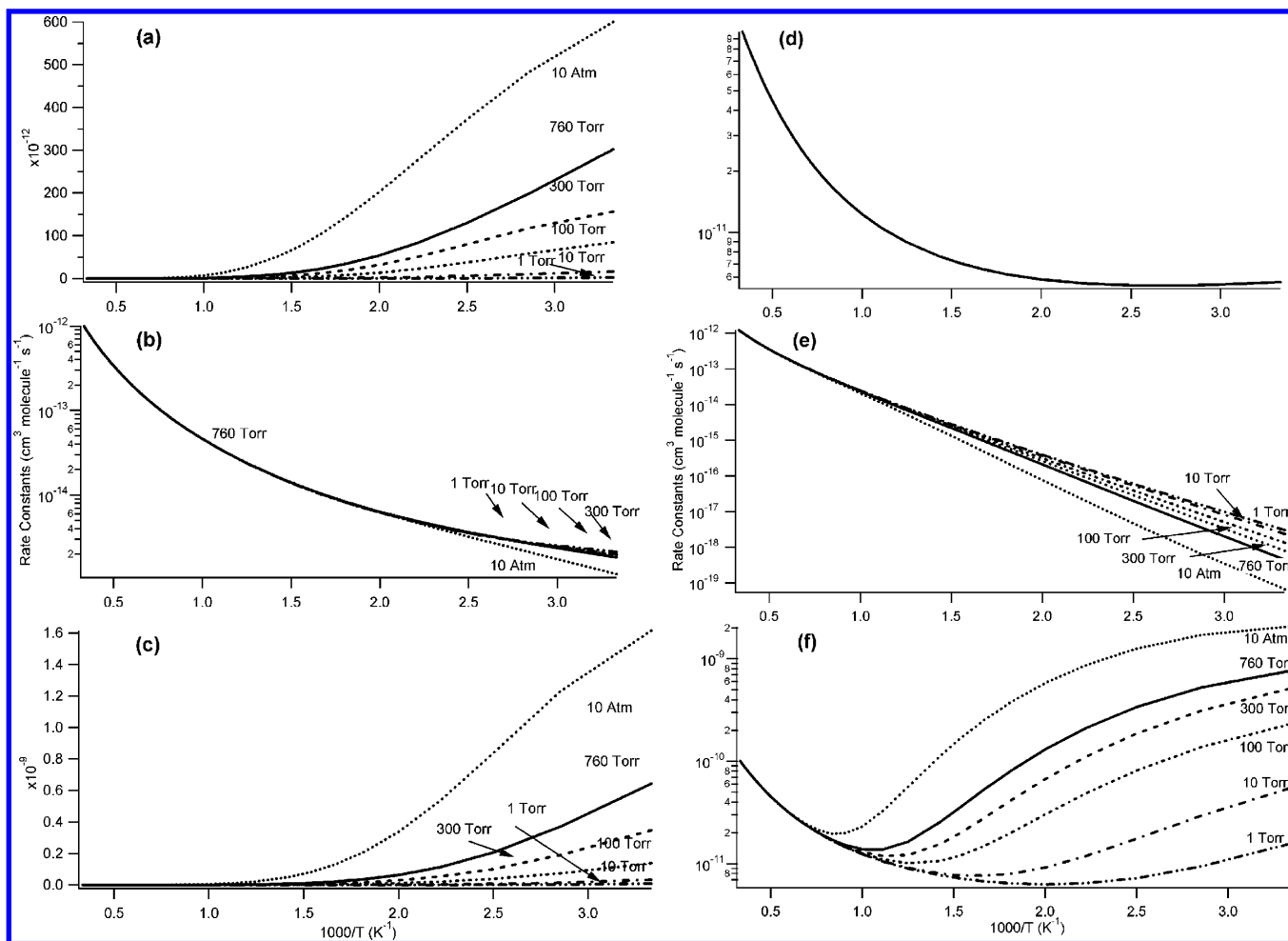


**Figure 4.** Predicted rate constants of  $k_1$  (a),  $k_2$  (b),  $k_4$  (c),  $k_9$  (e), and  $k_{total}$  (f) at Ar pressures of 1 Torr, 10 Torr, 100 Torr, 300 Torr, 760 Torr, and 10 atm, and  $k_7$  (d) at a high-pressure limit in the temperature range of 300–3000 K.

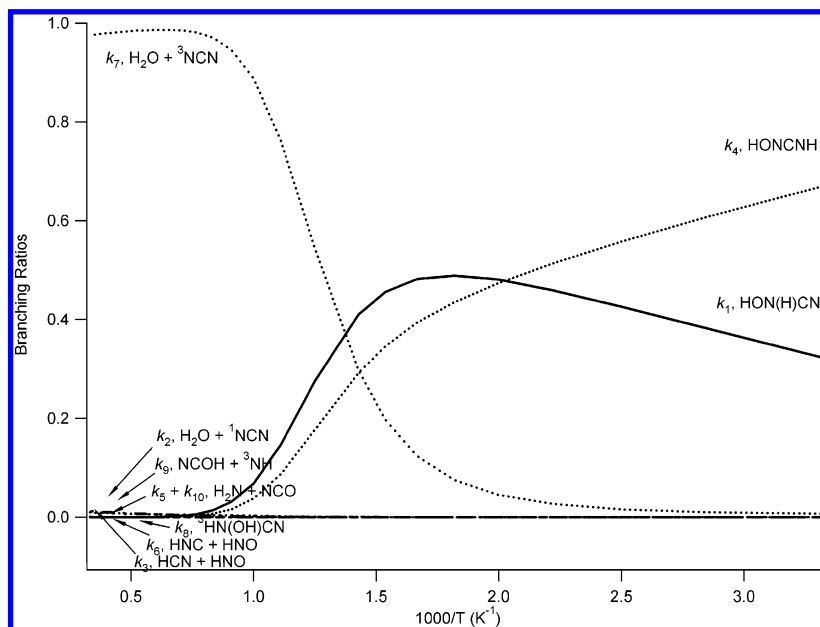


**Figure 5.** Predicted branching ratios for the 10 primary singlet and triplet reaction channels of the reaction OH + HNCN at 760 Torr Ar pressure in the temperature range of 300–3000 K.

integration over the energy range, an energy grain size of  $100 \text{ cm}^{-1}$  was used. The total angular momentum  $J$  covered the range from 1 to 250 in steps of 10 for the  $E, J$ -resolved calculation. The Morse potentials with the above-mentioned parameters, the Lennard-Jones pairwise potential, and the

anisotropic potential are added together to form the final potential, similar to that employed in the OH +  $CH_2O$ ,<sup>9</sup> OH +  $CH_3OH$ , and OH +  $C_2H_5OH$  reactions.<sup>17</sup>

The tunneling effect on the transition states— $TS_1$  and  $TS_2$  in channel 2,  $TS_{18}$  and  $TS_3$  in channel 3,  $TS_{16}$  in channel 5,  $TS_{13}$



**TABLE 2: Predicted Rate Expressions<sup>a</sup> of  $k_1, k_2, k_3, k_4, k_5, k_6, k_7, k_8, k_9, k_{10}$ , and  $k_{\text{total}}$  at Ar Pressures of 1, 10, 100, 300, 760, and 7600 Torr in the Temperature Range of 300–3000 K**

reaction	$P$ (Torr)	$A$	$n$	$B$	reaction	$P$ (Torr)	$A$	$n$	$B$	
$k_1$	1	$4.03 \times 10^{16}$	-10.14	-2144	$k_7$	1	$1.72 \times 10^{-19}$	2.48	949	
	10	$5.24 \times 10^{17}$	-10.17	-2284		10	$1.72 \times 10^{-19}$	2.48	949	
	100	$8.59 \times 10^{18}$	-10.22	-2549		100	$1.72 \times 10^{-19}$	2.48	949	
	300	$3.25 \times 10^{19}$	-10.24	-2730		300	$1.72 \times 10^{-19}$	2.48	949	
	760	$9.08 \times 10^{19}$	-10.24	-2905		760	$1.72 \times 10^{-19}$	2.48	949	
	7600	$7.22 \times 10^{20}$	-10.19	-3431	7600	$1.72 \times 10^{-19}$	2.48	949		
$k_2$	1	$3.93 \times 10^{-23}$	2.99	174	$k_8$	1	$2.86 \times 10^{13}$	-9.55	-3532	
	10	$4.85 \times 10^{-23}$	2.97	143		10	$3.25 \times 10^{14}$	-9.54	-3943	
	100	$4.96 \times 10^{-23}$	2.97	143		100	$1.40 \times 10^{15}$	-9.39	-3363	
	300	$5.44 \times 10^{-23}$	2.95	133		300	$1.42 \times 10^{15}$	-9.23	-4712	
	760	$6.91 \times 10^{-23}$	2.92	102		760	$8.33 \times 10^{14}$	-9.03	-4897	
	7600	$4.63 \times 10^{-22}$	2.69	173	7600	$1.44 \times 10^{13}$	-8.19	-5165		
$k_3$	1	$9.16 \times 10^{-16}$	0.74	-6749	$k_9$	1	$3.38 \times 10^{-18}$	1.72	-2965	
	10	$9.16 \times 10^{-16}$	0.74	-6749		10	$7.52 \times 10^{-18}$	1.62	-3104	
	100	$9.16 \times 10^{-16}$	0.74	-6749		100	$5.27 \times 10^{-17}$	1.39	-3455	
	300	$9.16 \times 10^{-16}$	0.74	-6749		300	$2.65 \times 10^{-16}$	1.19	-3760	
	760	$9.16 \times 10^{-16}$	0.74	-6749		760	$1.49 \times 10^{-15}$	1.00	-4105	
	7600	$9.09 \times 10^{-16}$	0.74	-6749	7600	$1.00 \times 10^{-13}$	0.51	-5172		
$k_4$	1	$1.47 \times 10^{12}$	-9.02	-656	$k_{10}$	1	$8.47 \times 10^{-16}$	0.74	-3102	
	10	$1.04 \times 10^{15}$	-9.54	-1298		10	$1.84 \times 10^{-15}$	0.65	-3225	
	100	$3.41 \times 10^{17}$	-9.95	-1896		100	$4.52 \times 10^{-14}$	0.27	-3862	
	300	$9.11 \times 10^{17}$	-9.93	-1949		300	$3.95 \times 10^{-13}$	0.11	-4329	
	760	$3.11 \times 10^{19}$	-10.25	-2345		760	$2.21 \times 10^{-12}$	-0.18	-4768	
	7600	$4.09 \times 10^{20}$	-10.26	-2755	7600	$1.36 \times 10^{-11}$	-0.36	-5780		
$k_5$	1	$2.56 \times 10^{-33}$	5.51	342	$k_{\text{total}}^b$	$T_1$	$2.16 \times 10^{-26}$	4.59	2405	
	10	$2.15 \times 10^{-31}$	4.98	-326		$T_2$	$1.48 \times 10^{-18}$	2.24	520	
	100	$9.86 \times 10^{-31}$	4.79	-549		$T_1$	$6.86 \times 10^{-29}$	5.26	3393	
	300	$1.34 \times 10^{-30}$	4.76	-592		$T_2$	$1.32 \times 10^{-18}$	2.25	537	
	760	$1.73 \times 10^{-30}$	4.72	-629		$T_1$	$1.05 \times 10^{-16}$	1.30	2216	
	7600	$6.57 \times 10^{-30}$	4.56	-822		$T_2$	$6.54 \times 10^{-19}$	2.33	697	
$k_6$	1	$3.15 \times 10^{-29}$	4.60	-4778		100	$T_1$	$1.56 \times 10^{-7}$	-1.61	1104
	10	$8.59 \times 10^{-29}$	4.48	-4917		$T_2$	$1.76 \times 10^{-19}$	2.48	996	
	100	$1.03 \times 10^{-28}$	4.45	-4942		300	$T_1$	$2.66 \times 10^2$	-4.50	-239
	300	$1.08 \times 10^{-28}$	4.45	-4949		$T_2$	$1.38 \times 10^{-20}$	2.78	1578	
	760	$1.13 \times 10^{-28}$	4.44	-4955	760	$T_1$	$1.23 \times 10^{15}$	-8.31	-2189	
	7600	$1.53 \times 10^{-28}$	4.41	-4998	$T_2$	$2.76 \times 10^{-27}$	4.56	5189		

<sup>a</sup> Rate constants are represented by  $k = AT^n \exp(B/T)$  in units of  $\text{cm}^3 \text{ molecule}^{-1} \text{ s}^{-1}$ . <sup>b</sup>  $T_1$ , temperature range of 300–1000 K;  $T_2$ , temperature range of 1000–3000 K.

in channel 6, and t-TS<sub>2</sub>, t-TS<sub>3</sub>, t-TS<sub>4</sub>, t-TS<sub>7</sub>, and t-TS<sub>8</sub> in channels 8, 9, and 10—are considered because their barriers are much higher than those of the reactants.<sup>9,17</sup> In this study, the tunneling effects are treated using Eckart's tunneling corrections.

Finally, HON(H)CN, HONCNH, TS<sub>18</sub>, and TS<sub>3</sub> in channel 3, TS<sub>16</sub> in channel 5, and TS<sub>13</sub> in channel 6 have their own optical isomers, so a statistical factor of 2 is employed in these rate constant calculations.

**2b. Predicted Rate Constants.** The predicted values for  $k_1$  forming singlet HON(H)CN at six specific pressures between 1 and 7600 Torr in the temperature range of 300–3000 K are shown in Figure 4 a and are also listed in Table 2. The values of  $k_1$  decrease with increasing temperature from 300 to 3000 K. In addition,  $k_1$  has a strong pressure dependence in the temperature range below 1000 K, as one expects. When the pressure increases from 1 Torr to 10 atm,  $k_1$  increases, as clearly illustrated by Figure 4a and the results listed in Table 2.

The predicted results for  $k_2$  producing  $\text{H}_2\text{O} + {}^1\text{NCN}$  products at six specific pressures between 1 and 7600 Torr in the temperature range of 300–3000 K are shown in Figure 4b and are also listed in Table 2.  $k_2$  is the sum of contributions from the reactions via TS<sub>1</sub> and TS<sub>2</sub>, in which the rate constants from the contribution via TS<sub>1</sub> account for 0.96–0.53 in the temperature range of 300–3000 K. The properties of  $k_2$  are completely different from those of  $k_1$ .  $k_2$  increases with increasing temperature from 300 to 3000 K; it has a weak pressure dependence

only at temperatures below 500 K due to competition with  $k_1$  resulting from collisional deactivation of the excited HON(H)CN.

The predicted values for  $k_4$  forming singlet HONCNH at six specific pressures between 1 and 7600 Torr in the temperature range of 300–3000 K are shown in Figure 4c and are also listed in Table 2.  $k_4$  as an association process has pressure/temperature (P,T) dependences similar to those of  $k_1$ .  $k_4$  decreases with increasing temperature from 300 to 3000 K. In addition,  $k_4$  also has a strong pressure dependence in the temperature range below 1000 K, as does  $k_1$ . When the pressure increases from 1 Torr to 10 atm,  $k_4$  increases, as clearly illustrated by Figure 4c and the results listed in Table 2.

The predicted pressure-independent values for  $k_7$ , producing  $\text{H}_2\text{O} + {}^3\text{NCN}$  in the temperature range of 300–3000 K, are shown in Figure 4d and are also listed in Table 2.  $k_7$  is an abstraction process by the triplet precomplex  ${}^3\text{OH}\cdots\text{N}(\text{H})\text{CN}$  and the transition state t-TS<sub>1</sub>. The properties of  $k_7$  are completely different from those of  $k_1$ ,  $k_2$ , and  $k_4$  because of the absence of pressure effect on this abstraction process.

The predicted results for  $k_9$  producing the products of  $\text{CNOH} + {}^3\text{NH}$  at six specific pressures between 1 and 7600 Torr in the temperature range of 300–3000 K are shown in Figure 4e and are also listed in Table 2.  $k_9$  is the sum of contributions from the reactions via t-TS<sub>4</sub> and t-TS<sub>7</sub>, in which the rate constants from the process via t-TS<sub>4</sub> account for 0.13–0.49 in

the temperature range of 300–3000 K.  $k_9$  as an dissociation process is similar to  $k_2$ .  $k_9$  increases with increasing temperature from 300 to 3000 K; it is pressure-dependent at temperatures below 1000 K.

The predicted total rate constants for  $k_{\text{total}} = k_1 + k_2 + k_3 + k_4 + k_5 + k_6 + k_7 + k_8 + k_9 + k_{10}$  at 10 specific pressures between 1 and 7600 Torr in the temperature range 300–3000 K are shown in Figure 4f and listed in Table 2. The P,T dependences of  $k_{\text{total}}$  are closely parallel with those of  $k_1$  and  $k_4$  in the temperature range below about 1000 K.  $k_{\text{total}}$  decreases with increasing temperature from 300 to about 1000 K and also has a strong pressure dependence in the temperature range below 1000 K. However, with temperature over 1000 K, the property of  $k_{\text{total}}$  is close to that of  $k_7$ ; it increases upon increasing temperature from 1000 to 3000 K. In comparison, the values of  $k_{\text{total}}$  in the lower temperature range are still higher than those in the higher temperature range due to dominant  $k_1$  and  $k_4$  through collisional deactivation.

The predicted individual rate constants given in units of molecules per cubic centimeter and time in seconds ( $\text{cm}^3 \text{molecule}^{-1} \text{s}^{-1}$ ) at a 760 Torr Ar pressure in the temperature range 300–3000 K can be represented by

$$k_1 = 9.08 \times 10^{19} \times T^{-10.24} \exp(-2905/T)$$

$$k_2 = 6.91 \times 10^{-23} \times T^{2.92} \exp(102/T)$$

$$k_3 = 9.16 \times 10^{-16} \times T^{0.74} \exp(-6749/T)$$

$$k_4 = 3.11 \times 10^{18} \times T^{-10.25} \exp(-2345/T)$$

$$k_5 = 1.73 \times 10^{-30} \times T^{4.72} \exp(-629/T)$$

$$k_6 = 1.13 \times 10^{-28} \times T^{4.44} \exp(-4955/T)$$

$$k_7 = 1.72 \times 10^{-19} \times T^{2.48} \exp(949/T)$$

$$k_8 = 8.33 \times 10^{14} \times T^{-9.03} \exp(-4897/T)$$

$$k_9 = 1.49 \times 10^{-15} \times T^{1.00} \exp(-4105/T)$$

$$k_{10} = 2.21 \times 10^{-12} \times T^{-0.18} \exp(-4767/T)$$

The total rate constants at 760 Torr of Ar pressure can be represented by two fitting equations:  $k_{\text{total}} = 2.66 \times 10^2 \times T^{-4.50} \exp(-239/T)$  at  $T = 300$ – $1000$  K and  $1.38 \times 10^{-20} \times T^{2.78} \exp(1578/T) \text{ cm}^3 \text{ molecule}^{-1} \text{ s}^{-1}$  at  $T = 1000$ – $3000$  K. At present, no comparison can be made for the calculated and experimental data. For this newly identified, potentially important, prompt NO precursor reaction, our results are recommended for high-temperature combustion modeling applications.

**2c. Predicted Branching Ratios.** The branching ratios of the rate constants  $k_1$ – $k_6$  at an Ar pressure of 760 Torr in the temperature range of 300–3000 K are shown in Figure 5.  $k_1$  accounts for 0.32–0.28 and  $k_4$  accounts for 0.68–0.17 in the temperature range of 300–800 K.  $k_7$  accounts for 0.55–0.98 in the high-temperature range of 800–3000 K. Because both  $k_2$  and  $k_7$  can produce  $\text{H}_2\text{O}$ , and excited  $^1\text{NCN}$  from  $k_1$  can transfer to its ground state  $^3\text{NCN}$  finally, the total branching ratios of  $\text{H}_2\text{O}$  and  $\text{NCN}$  with the sum of  $k_2$  and  $k_7$  account for 0.55–0.99 in the high-temperature range of 800–3000 K. The branching ratios of  $k_3$  for producing  $\text{HCN} + \text{HNO}$ ,  $k_6$  for producing  $\text{H}_2\text{N} + \text{NCO}$ ,  $k_8$  for forming  $^3\text{HN}(\text{OH})\text{CN}$ ,  $k_9$  for

producing  $\text{CNOH} + ^3\text{NH}$ , and  $k_5 + k_{10}$  for producing  $\text{NH}_2$  and  $\text{NCO}$  are negligible, even in the higher temperature range. Therefore, the singlet primary intermediates,  $\text{HON}(\text{H})\text{CN}$  and  $\text{HONCNH}$ , are expected to be stable in the low-temperature range and begin to dissociate when temperature is over 800 K, producing  $\text{H}_2\text{O}$  and  $\text{NCN}$  as the primary products.

## Conclusions

The kinetics and mechanism for the OH + HNCN reaction with singlet and triplet PESs have been studied at the CCSD-(T)/6-311+G(3df,2p)//B3LYP/6-311+G(3df,2p) and CCSD/6-311++G(d,p) levels of theory. The total and individual rate constants for the primary channels of the reaction in the temperature range of 300–3000 K are predicted. The primary intermediates formed—singlet  $\text{HON}(\text{H})\text{CN}$  and  $\text{HONCNH}$ —are stable in the low-temperature range and begin to dissociate when temperature is higher than 800 K, giving rise to  $\text{H}_2\text{O}$  and  $\text{NCN}$  as the primary products through the singlet and triplet PESs of the OH + HNCN reaction. Our predicted total and individual rate constants and product branching ratios for this critical reaction may be employed for combustion kinetic modeling applications.

**Acknowledgment.** The authors are grateful for the support of this work from the Basic Energy Sciences, Department of Energy, under Contract No. DE-FG02-97-ER14784. M.C.L. acknowledges the support from the National Science Council of Taiwan for a distinguished visiting professorship and the Taiwan Semiconductor Manufacturing Company for the TSMC Distinguished Professorship.

**Supporting Information Available:** **Table S1:** Cartesian coordinates of the optimized geometries of intermediates and transition states of the reaction OH + HNCN at the B3LYP/6-311+G(3df,2p) and CCSD/6-311++G(d,p) levels. **Table S2:** The frequencies and moments of inertia of the optimized geometries of the reaction OH + HNCN at the B3LYP/6-311+G(3df,2p) and CCSD/6-311++G(d,p) levels. **Figure S1.** The whole PES of the reaction OH + HNCN calculated at the CCSD(T)/6-311+G(3df,2p)//B3LYP/6-311+G(3df,2p) levels. This material is available free of charge via the Internet at <http://pubs.acs.org>.

## References and Notes

- (1) Herzberg, G.; Travis, D. N. *Can. J. Phys.* **1963**, *41*, 286.
- (2) Wu, M.; Hall, G.; Sears, T. J. *J. Chem. Soc., Faraday Trans.* **1993**, *89*, 615.
- (3) Yamamoto, S.; Saito, S. *J. Chem. Phys.* **1994**, *101*, 10350.
- (4) Clifford, E. P.; Wenthold, P. G.; Lineberger, W. C.; Petersson, G.; Ellison, G. B. *J. Phys. Chem. A* **1997**, *101*, 4338.
- (5) Bise, R. T.; Hoops, A. A.; Neumark, D. M. *J. Chem. Phys.* **2001**, *114*, 9000.
- (6) Tao, F.-M.; Klemperer, W.; Thaddeus, P. *J. Chem. Phys.* **1994**, *100*, 3691.
- (7) Puzzarini, C.; Gambi, A. *J. Chem. Phys.* **2005**, *122*, 064316.
- (8) Moskaleva, L. V.; Xia, W. S.; Lin, M. C. *Chem. Phys. Lett.* **2000**, *331*, 269.
- (9) Xu, S. C.; Zhu, R. S.; Lin, M. C. *Int. J. Chem. Kinet.* **2006**, *28*, 322.
- (10) Klippenstein, S. J.; Wagner, A. F.; Dunbar, R. C.; Wardlaw, D. M.; Robertson, S. H. *VariFlex*, version 1.0; Argonne National Laboratory: Argonne, IL, 1999.
- (11) Frisch, M. J.; Trucks, G. W.; Schlegel, H. B.; Scuseria, G. E.; Robb, M. A.; Cheeseman, J. R.; Zakrzewski, V. G.; Montgomery, J. A., Jr.; Stratmann, R. E.; Burant, J. C.; Dapprich, S.; Millam, J. M.; Daniels, A. D.; Kudin, K. N.; Strain, M. C.; Farkas, O.; Tomasi, J.; Barone, V.; Cossi, M.; Cammi, R.; Mennucci, B.; Pomelli, C.; Adamo, C.; Clifford, S.; Ochterski, J.; Petersson, G. A.; Ayala, P. Y.; Cui, Q.; Morokuma, K.; Malick, D. K.; Rabuck, A. D.; Raghavachari, K.; Foresman, J. B.; Cioslowski, J.; Ortiz, J. V.; Baboul, A. G.; Stefanov, B. B.; Liu, G.; Liashenko, A.; Piskorz,

P.; Komaromi, I.; Gomperts, R.; Martin, R. L.; Fox, D. J.; Keith, T.; Al-Laham, M. A.; Peng, C. Y.; Nanayakkara, A.; Gonzalez, C.; Challacombe, M.; Gill, P. M. W.; Johnson, B.; Chen, W.; Wong, M. W.; Andres, J. L.; Gonzalez, C.; Head-Gordon, M.; Replogle, E. S.; Pople, J. A. *Gaussian 98*, revision A.7; Gaussian, Inc.: Pittsburgh, PA, 2003.

(12) Martin, J. M. L.; Taylor, P. R.; Francois, J. P.; Gijbels, R. *Chem. Phys. Lett.* **1994**, *226*, 475.

(13) Bise, R. T.; Choi, H.; Neumark, D. M. *J. Chem. Phys.* **1999**, *111*, 4923.

(14) Taylor, T. R.; Bise, R. T.; Asmis, K. R.; Neumark, D. M. *Chem. Phys. Lett.* **1999**, *301*, 413.

(15) Ruscic, B.; Boggs, J. E.; Burcat, A.; Csaszar, A. G.; Demaison, J.; Janoschek, R.; Martin, J. M. L.; Morton, M. L.; Rossi, M. J.; Stanton, J. F.; Szalay, P. G.; Westmoreland, P. R.; Zabel, F.; Berces, T. *J. Phys. Chem. Ref. Data* **2005**, *34*, 573.

(16) Chase, M. W., Jr. *NIST-JANAF Thermchemical Tables*, 4th ed.; J. Phys. Chem. Ref. Data, Monograph 9; Woodbury, NY, 1998; p 1.

(17) Xu, S. C.; Lin, M. C. *Proc. Combust. Inst.* **2007**, *31*, 159.

(18) Gilbert, R. G.; Smith, S. C. *Theory of Unimolecular and Recombination Reactions*; Blackwell Scientific: Oxford, 1990.